TECHNICAL CONSIDERATIONS IN THE USE OF A GAMMA CAMERA 1,600-CHANNEL ANALYZER SYSTEM FOR THE MEASUREMENT OF REGIONAL CEREBRAL BLOOD FLOW

Wolf-Dieter Heiss, Pius Prosenz, and Alexander Roszuczky

Neurologische Universitätsklinik, Vienna, Austria

Scintillation cameras, especially the gamma camera developed by Anger (*1*), have become an important tool for the visualization of organs. Recently they have also been applied in dynamic studies making use of the speed of the system in registering and localizing the distribution of radioactivity in two dimensions. For a quantitative measurement it is necessary to store the gamma-camera data; computer-oriented systems are the most advantageous for this purpose (*2*). The output of the scintillation camera is either recorded on analog magnetic tape and subsequently quantitatively analyzed by various photoelectric means (*3,4*), or a multichannel analyzer may be used from which data collected over short periods of time are transferred into a store (*5*); further off-line processing is carried out on a digital computer (*6*).

The gamma camera was used by Heiss, et al (*7,8*) with a 1,600-channel analyzer and a digital magnetic tape system in combination with a computer for the measurement of regional cerebral blood flow (rCBF). A similar approach to rCBF measurement was made by Potchen, et al (*9*), using the gamma camera in connection with a small on-line computer. However, the gamma-camera technique is not yet fully accepted as a method for measuring rCBF; the differences from single-detector systems have been critically discussed (*10–12*). The purpose of this paper is to investigate and describe some important properties, such as efficiency, energy resolution, and deadtime of the system used; some possibilities for correcting or minimizing the errors which result from low count rates are outlined.

MATERIALS

For the measurement of cerebral blood flow (CBF), ^{133}Xe in saline solution is injected into the internal carotid artery and the washout of the isotope is recorded over the intact skull (*13,14*). Our equipment consists of three interconnected units:

1. Sampling and localization of information were achieved by a scintillation camera (Nuclear-Chicago, Pho/Gamma III). The operational details and physical characteristics of the Anger-type camera have been dealt with in several papers (*1,15–17*).
2. The analog impulses provided by the camera are converted into digital form (dual ADC, RIDL Model 22-3) and stored in an address proportional to their amplitude in the 1,600-word memory (RIDL, Model 24-3). The investigator may choose the size of the crystal area which collects impulses for one channel in the memory. Storage periods are preset by a crystal-driven clock, which automatically starts another sampling period after having dumped the memory.
3. Impulses accumulated during sampling periods of 2.4 sec for the first 2 min after intracarotid Xe injection and of 18 sec during the following 8 min are stored by means of a digital magnetic tape system (Nuclear-Chicago Model 2402, Interface and Ampex TM 9). 1,600 words, size 10^3 each, are transferred from the memory to the tape in 0.3 sec. Computer compatibility is obtained by use of a packing density of 800 bits/in. The data are processed off-line by an IBM 1800 data-acquisition and control system and the results are printed out in the form of rCBF maps.

EFFICIENCY AND ANALYSIS OF IMPULSE ENERGY

The energy resolution of scintillation cameras has already been discussed by various authors (*15,18–20*). The efficiency of gamma-ray detection is limited at low energy by absorption in the aluminum

Received July 14, 1971; revision accepted Feb. 28, 1972.

For reprints contact: W. D. Heiss, Hirnkreislauflaboratorium, Neurologische Universitätsklinik, Spitalgasse 23, Vienna, Austria.

plates covering the collimator (1.6 mm) and the crystal (0.8 mm). For photons of high energy the efficiency decreases gradually with increasing energy. The efficiency has its maximum at 100 keV and is 84% for ^{99m}Tc. ^{133}Xe has its main photopeak at 81 keV, and a second peak at 31 keV caused by x-rays from the K shell. Using a discriminator setting at 81 keV with a window of ±17.5%, the calculated photopeak efficiency of the system used is 86% for ^{133}Xe.

In order to monitor the energy distribution of the radiation and to check the influence of scatter, spectra were obtained from the gamma camera by feeding the Z-impulse output into the pulse-height analyzer and taking a picture of the pulse-height distribution. These studies gave useful guidance for the proper setting of the discriminator.

The height of the x-ray peak at 31 keV, shown by Crouthamel (*21*) to be 167% of the height of the 81-keV peak, is decreased in the system used to 54% of the height of the 81-keV peak because of the absorption in the aluminum plates on the crystal and the collimator (Fig. 1B). In the measurement of CBF, absorption also takes place within the skull (*22*). However, the degree of absorption is not constant during a study. As may be seen in Fig. 1C, the 31-keV x-ray peak is very low in a spectrum taken during the first 40 sec of a CBF study, as long as the isotope is present in the brain only. Due to recirculation an increasing amount of the isotope is washed into scalp and skull. As the radiation from superficial layers becomes more and more intense, the percentage of low-energy rays in the total count rate rises (Fig. 1D). Consequently, the error of the flow values, especially when calculated according to the height-over-area formula, may well be accentuated when the discriminator is set at 25 keV, thereby including the 31-keV peak.

The presence of lead in the collimator results in a high incidence of *low-energy L-shell and M-shell x-rays*. With high count rates, sum peaks caused by two or more low-energy pulses are more and more likely. They may fall in the energy range above 20 keV (*23*).

Compton interactions of low-energy photons (e.g., 81 keV) result in only a slight loss of energy to the recoil electron, and therefore the energies of primary and scattered photons differ only slightly, as evident from a comparison of Fig. 1C and D. Consequently scattered radiation originating from low-energy photons cannot be eliminated completely. This is especially important for voluminous radiating sources, such as brain and liver, where more gamma-ray scattering occurs than in thin radiating layers

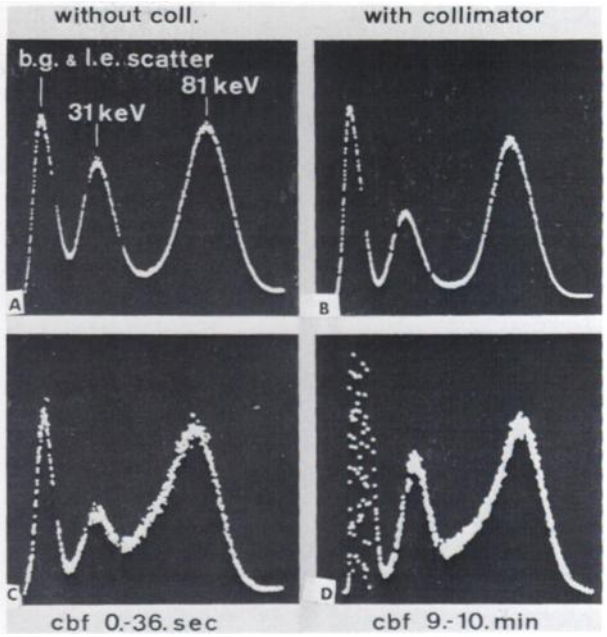

FIG. 1. Spectra of ^{133}Xe obtained by using gamma camera as simple detector and 1,600-word memory as pulse-height analyzer. Attenuation of the 31-keV peak by collimator and its aluminum plate may be seen by comparing spectra obtained with and without collimator. Comparison of spectra recorded during cerebral blood flow (CBF) study with spectra of xenon sources gives some information about incidence of scatter. During first 36 sec of CBF study, 31-keV peak is very small, due to low penetration ability of this radiation. With higher recirculation and appearance of isotope in scalp and skull, 31-keV peak increases, resulting in additional error caused by low level discrimination. B.g. & l.e. scatter is electronic background and low-energy (x-ray) scatter.

(*24–26*). Compton interactions may also occur within the crystal (*27,28*).

The contribution of Compton scatter to the pulse-height spectrum was assessed by comparing spectra of ^{133}Xe recorded under different experimental conditions. The spectra in Fig. 1A and B were obtained by viewing the isotope without scattering media between collimator and source. This is the pulse-height spectrum of the system for the primary x and gamma rays from ^{133}Xe. The spectra in Fig. 1C and D were recorded while observing the washout of ^{133}Xe from the brain; they show the sum of the spectra of primary and scattered radiation. According to Potchen, et al (*26*), up to 55% of the total radiation seen by the probe may not come from the geometric area under the probe. If all energies from below 31 keV to above 81 keV are included, as is usually done in multidetector techniques (*11,12*), or if the discriminator is set at 50 keV (*29*), about 50% of the number of pulses is contributed by Compton scatter. This percentage is lowered to 13% with an optimal discriminator setting at 75 keV (*26*). The discriminating window in the gamma camera (81 keV ± 17.5%) reduced the recorded Compton scatter to 30%. This 30% of scattered radiation with an energy close to that of the primary photon

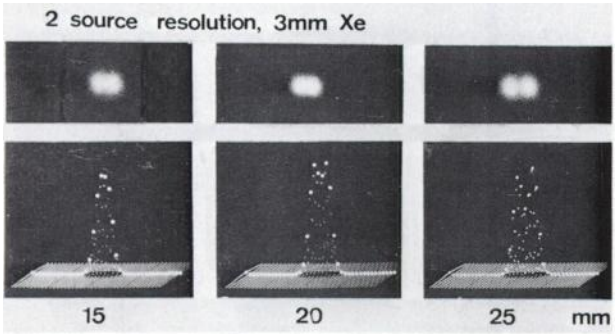

FIG. 2. Spatial resolution of two 3-mm xenon sources represented as pictures from gamma-camera oscilloscope and from 1,600-word memory display. Profile lines through peaks of activity show their discernibility.

results from collisions with a small angle of deflection (*24,30*) and does not substantially impair the target/nontarget ratio. The proportion of off-target rays seen by the crystal is further reduced by the use of a special multichannel collimator for gamma-ray energies under 200 keV. This was shown in spectra recorded from a well-collimated 3-mm Xe source directed at various angles of incidence through a scattering medium (paraffin hemisphere with a radius of 70 mm). Slight shifts of 15 deg from the axis caused a substantial decrease of both primary radiation and Compton scatter; with a 30-deg deflection, no radiation with an energy above the secondary x-rays was detectable.

SPATIAL RESOLUTION

Crucial for the spatial resolution of the whole system is the inherent position resolution of the image detector, which is composed of the crystal, light pipe, and photomultiplier combination. A scintillation in the crystal gives rise to an isotropic light distribution within the plane of the phototubes, which limits the inherent resolution (*31*). The statistical spreading of coordinate pulses in the photomultipliers is a further disturbing factor (*18,32*).

The inherent resolution of the detector without collimator was estimated with the "absorber bar pattern" (*15*), using a phantom with ⅛-in.-thick lead bars having a width of ¼, ⅜, ½, and ¾ in. and separated by equivalent spaces. One-fourth-in. intervals (= 6.35 mm) were discernible with a ^{99m}Tc source.

For our blood-flow studies the special multichannel collimator for gamma-ray energies under 200 keV was used. This has a theoretical spatial resolution of 6.25 mm, which corresponds well to the inherent resolution shown with the absorber bar phantom. The stability and the linearity of the electronic network and of the display (*16*), as well as the analog-to-digital conversion are sufficiently accurate and have no deteriorating influence on the spatial resolution. The resolving capacity described above determined us to coordinate one channel in the 1,600-word memory to a crystal area of 6 × 6 mm.

As one means of estimating the spatial resolution of the whole system the two-sources method (*28, 33*) was used. Spatial resolution was expressed in digital terms according to the differences in the content of adjacent channels of the core memory. With the chosen correspondence of 6 × 6-mm areas of the crystal to individual channels, the resolution was tested using Xe sources with a diameter of 3 mm (Fig. 2). Two sources 20 mm apart could be distinguished optically on the oscilloscope and on the 1,600-word memory by a valley in count rates; at a distance of 25 mm between the sources 3 channels showing lower count rates separated the maxima. These results confirmed previous investigations using two ^{241}Am sources (photopeak at 60 keV) with diameters of 1–2 mm and with two ^{133}Xe sources with diameters of 2 mm (*8*).

The resolution was further examined using the concept of full width at half maximum (FWHM) height (*20,34*). Spatial distribution functions were obtained in the multichannel analyzer in the CBF measuring condition using Xe sources with diameters of 2 and 3 mm in direct contact with the crystal window (2 mm diam: FWHM = 15 mm; 3 mm diam: Fig. 3A, FWHM = 19 mm), separated from the crystal by 40-mm paraffin (3-mm source: Fig. 3B, FWHM = 28 mm), in direct contact with the collimator surface (2-mm source: FWHM = 16 mm; 3-mm source: Fig. 3C, FWHM = 20 mm), and separated from the collimator by 40-mm paraffin (3-mm source: Fig. 3D, FWHM = 21 mm). The comparison of Fig. 3C and D demonstrates only slight deterioration of the resolution with increasing distance of sources from the crystal and with increasing influence of scattering media. These findings are in agreement with other investigations (*19,20,32, 34,35*) and show a good correlation to the resolution values obtained with the method of two point sources.

A comparison of the resolution of the gamma-camera 1,600-word memory system and of the multiprobe technique is difficult, because reported investigations of the multiprobe technique do not exhaustively deal with the problem of scatter and do not use accepted definitions. Usually a cylindrical nonfocusing collimator is used for multidetector studies of regional blood flow. Some authors (*11,13*) assume that the tissue region from which one detector receives its pulses is represented by the volume inside a truncated cone through the center of the surface of the crystal and through the opening of

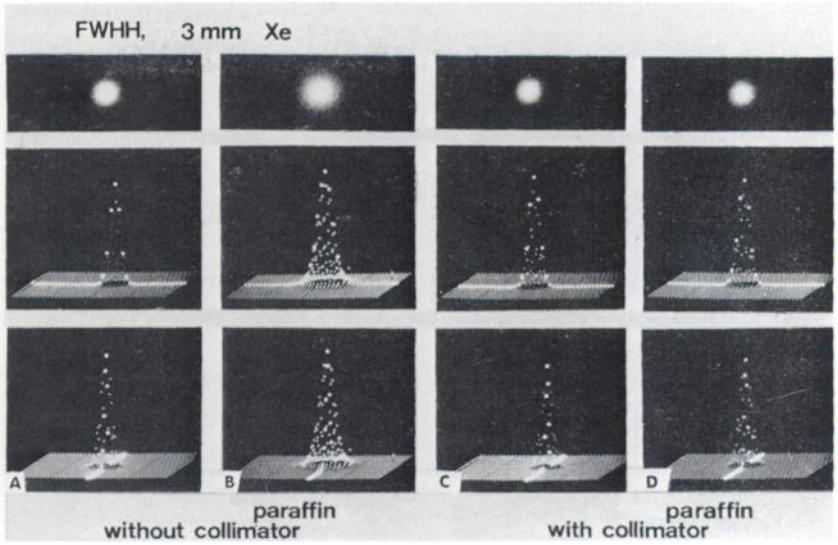

FIG. 3. Spatial resolution of 3-mm xenon sources represented as spots on gamma-camera oscilloscope and as distribution function obtained from 1,600-word memory. Without collimator: source close to crystal surface, FWHM = 19 mm; source separated by 40 mm paraffin, FWHM = 28 mm. With collimator, source close to collimator surface, FWHM = 20 mm; source separated by 40 mm paraffin, FWHM = 21 mm.

the collimator. But, as Paulson, et al (*11*) themselves stated, the tissue inside the truncated cone accounts for only approximately 65% of the counts; the figures obtained by Wilkinson, et al (*36*) with phantom studies were even worse and necessitated a modification of the collimator. Lassen and Ingvar (*12*), using 32 or 35 individual ¼-in. scintillation crystals, specify the two-dimensional resolution at a plane 3 cm from the surface of the collimator as 2 cm and define this resolution as follows: "50% of counts coming from this plane originate within a circle with a diameter of 2 cm". Apparently the effect of intermediate scattering tissue (skull, etc.) is not expressed in this figure. The overlapping between neighboring regions is mentioned (*11*), but no details are given.

The gamma-camera 1,600-word memory system used for the measurement of rCBF gave an effective resolution of 15–20 mm for ^{133}Xe, as determined by three different methods. This value is in agreement with other studies (see, for example, Refs. *15,19,20,32,35*). With respect to spatial resolution this system is superior to the single-probe technique.

DEADTIME, COUNT LOSS, AND COUNTING STATISTICS

Deadtime. The deadtime of the scintillation camera 4.5 μsec) is increased by connecting the 1,600-word memory, because the impulses are fed to the ADC by a delay network. The sum of original deadtime plus delay is the valid deadtime (11 μsec) for the gamma-camera scaler in the configuration used. The processing time (P) within the 1,600-word memory depends on the amplitudes of simultaneously processed x and y impulses and is calculated according to: $P = A + B + C\ (N + 10)$ (A: converter coincidence logic time, 6 μsec; B: transfer time, 4 μsec; C: 0.25 μsec/channel for 4-MHz digitizing rate; N: channel number in x or y coordinate). P is added to the deadtime of the camera. The total deadtime for pulses in the center of the 40 × 40 matrix amounts to 23 μsec.

The deadtimes of the scintillation camera and of the camera connected to the 1,600-word memory as specified by the manufacturers were checked by means of a 1-kHz double-pulse generator. In order to obtain actual deadtimes the values were re-examined with statistically distributed count rates using the multisource method with the sources at the center of the field of view.

Count loss. Statistically distributed count rates, as registered from a radiating source, suffer a count loss, which is negligible at low count rates but increases more than linearly with increasing count rate. The number (N_R) of counts recorded during time (T) is calculated from the total number (N) of impulses offered and the deadtime (τ) for processing of one impulse according to the widely used formula (see, for example, Refs. *37,38*)

$$N_R = \frac{N}{1 + \frac{N\tau}{T}}. \qquad (1)$$

For very high count rates some additional losses occur: Summing up of two photons arriving simultaneously or separated only by time periods shorter than the decay of the impulse produces a new impulse, which shows a higher energy and falls outside the discriminator window. With very high pulse rates the line of zero potential may not be reached after each impulse, and the baseline is shifted to a value above 0 volt, which results again in a reduction of the maximal count rates. These physical effects are inherent in all scintillation detecting systems with window discrimination.

Within a range from 10^2 to 8.8×10^4 cps the count loss in the system used was determined by

TABLE 1. COMPARISON OF NUMBER OF IMPULSES OFFERED† (N*) AND ERROR (ΔN*)‡ AND RECORDED COUNTS (N_R) WITHIN GAMMA CAMERA AND 1,600-WORD MEMORY||

Calculated number of impulses offered			Gamma-camera ($\tau = 11$ μsec) ($\Delta\tau = 0.161$ μsec)						1,600-word memory ($\tau = 23$ μsec) ($\Delta\tau = 0.161$ μsec)					
N*	ΔN*	(%)	N_R	(% loss)	$\sqrt{N_R}$	(%)	ΔN_R	(%)	N_R	(% loss)	$\sqrt{N_R}$	(%)	ΔN_R	(%)
661	25.7	3.89	656	0.6	25.6	3.91	25.3	3.86	651	1.4	25.5	3.92	24.9	3.84
1,161	34.1	2.94	1,147	1.1	33.9	2.96	33.2	2.90	1,131	2.5	33.6	2.98	33.2	2.94
3,741	61.2	1.64	3,594	3.9	59.9	1.67	56.4	1.57	3,445	7.9	58.7	1.70	51.9	1.51
6,730	82.7	1.23	6,267	6.9	79.2	1.26	71.4	1.13	5,511	18.1	76.2	1.35	61.8	1.12
10,002	102.6	1.03	9,011	9.1	94.9	1.05	82.2	0.91	8,132	18.7	90.2	1.11	67.0	0.82
15,002	132.8	0.88	12,878	14.2	113.5	0.88	94.1	0.73	11,154	25.6	105.6	0.95	70.6	0.63
23,288	196.3	0.84	18,539	20.4	136.2	0.73	111.4	0.60	15,165	34.9	123.1	0.81	74.6	0.49
32,212	296.6	0.92	23,786	26.2	154.2	0.65	133.6	0.56	18,505	42.6	136.0	0.74	80.4	0.44
57,961	829.3	1.43	35,397	38.9	188.1	0.53	220.7	0.62	24,844	57.1	157.6	0.63	108.7	0.44
88,864	1,821.0	2.05	44,939	49.4	212.0	0.47	333.7	0.74	29,195	67.1	170.9	0.59	140.9	0.48

† Calculated from Eq. 1.
‡ Calculated from Eq. 5.
|| Due to deadtime (τ) a pulse-rate dependent loss occurs. For the count rates used ($N_R < 15{,}000$ cps) the valid error of the recorded number of counts ΔN_R (calculated from Eq. 3) is smaller than the error N_R (calculated as the square root of the count number). Counting time for all values given is 1 sec.

three different methods: a multisource method, a 1:2 dilution series of Xe solutions, and by registering the decay of an area source of ^{99m}Tc (Fig. 4). These results agree well with calculations using Eq. (1) (Table 1). The curves obtained empirically as well as theoretically can be used for correction of count loss. This correction is necessary because the count loss is bigger at the high initial peak, which was 5,000–15,000 cps on the far left side of the curve in Fig. 4, than at the tail of the curve. All 70 values sampled during 10 min over every region (i.e., 50–100 12 × 12-mm areas in one hemisphere) were corrected for count loss. Carrying out this correction it was taken into consideration that the count loss depends on the count rate within the system (as shown in Fig. 4) as well as on the distribution of the coordinates of the pulses processed within the 1,600-word memory. Correction was accomplished off-line by an IBM-1800 data-acquisition and control system. To these basic data a washout curve composed of two monoexponential functions was fitted using the least-squares fit (Fig. 5). The rCBF values were computed using the stochastic and bicompartmental analyses (for details, see Ref. *39*).

Counting statistics. The variance of the number of registrations is not only dependent on the number of impulses, but is also influenced by the deadtime of the recording system (*40*). The number of impulses offered to the system as well as the deadtime for processing one impulse show statistical fluctuations, which must be considered when deriving the error of the number of registered counts.

For calculation purposes it may be assumed for our count rates that the distribution of the number

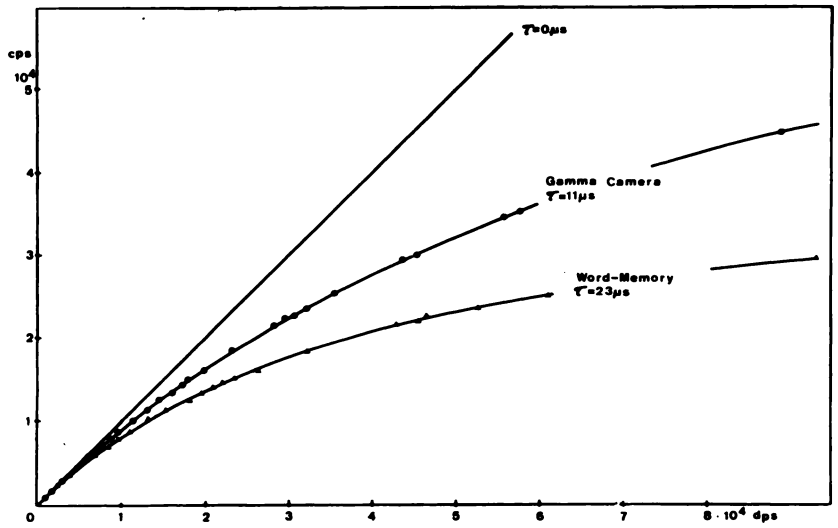

FIG. 4. Relation between number of offered impulses (abscissa, disintegrations per second) and number of recorded impulses (ordinate, counts per second) with deadtime of gamma camera and 1,600-word memory. Points shown were obtained by calculating offered impulses from recorded counts according to Eq. 1; validity of curves was checked by multisource method. Maximal count rates used are between 10,000 and 15,000 cps.

of pulses offered from a stable source in replicate measurements having a fixed observation time is a Gaussian curve (*38*). Consequently, the error (ΔN_R) of every recorded number (N_R) of counts affected by deadtime is given according to the law of error propagation (for derivation, see Ref. *41*) by

$$\Delta N_R = \sqrt{\left(\Delta N \frac{\partial N_R}{\partial N}\right)^2 + \left(\Delta\tau \frac{\partial N_R}{\partial \tau}\right)^2}. \quad (2a)$$

In a similar way the error (ΔN^*) of every calculated number (N^*) of offered impulses can be worked out:

$$\Delta N^* = \sqrt{\left(\Delta N_R \frac{\partial N^*}{\partial N_R}\right)^2 + \left(\Delta\tau \frac{\partial N^*}{\partial \tau}\right)^2}. \quad (2b)$$

The substitution of ΔN in Eq. 2a by $\sqrt{N}$, i.e., the relation for Gaussian distributed pulses (*38*), leads to

$$\Delta N_R = \frac{\sqrt{N + \frac{N^4\Delta\tau^2}{T^2}}}{\left(1 + \frac{N\tau}{T}\right)^2}. \quad (3)$$

τ represents the deadtime per impulse of the equipment, $\Delta\tau$ its error, and T the counting time.

With this error (ΔN_R) of the counted number of pulses one can calculate by the law of error propagation (Eqs. 1 and 2b) the number of pulses (N^*), which is practically identical with the number of offered impulses (N), and its error (ΔN^*), which is different from the statistical fluctuation ($\sqrt{N}$) of the offered impulses (N):

$$N^* \pm \Delta N^* = \frac{N_R}{1 - \frac{N_R\tau}{T}} \pm \frac{\sqrt{\Delta N_R^2 + \frac{N_R^4\Delta\tau^2}{T^2}}}{\left(1 - \frac{N_R\tau}{T}\right)^2}. \quad (4)$$

Substituting N_R by Eq. 1 and the error of the number of impulses counted in the measuring device by Eq. 3 one ends up with the following equation:

$$\Delta N^* = \sqrt{N^*}\sqrt{1 + 2\frac{N^{*3}\Delta\tau^2}{T^2}}. \quad (5)$$

It is evident from this equation that the error of the computed number (N^*) of impulses offered, for a given number (N_R) of counts recorded, is independent of the absolute value of the deadtime of the system; it only depends on the error of the deadtime ($\Delta\tau$). This is valid as long as the deadtime is independent of the count rate. This theoretical derivation is of high implication for the equipment used. The error calculated from measured count rates ($\sqrt{N_R}/N_R$) is not valid in cases of count loss caused by deadtime. As may be seen from Eqs. 1 and 3, the actual error of N_R is ΔN_R, which is smaller than $\sqrt{N_R}$ (Table 1). With the calculation of N^* from N_R, the error $\Delta N^*/N^*$ is bigger than the error $\Delta N_R/N_R$, but in our range (below 15,000 cps) markedly smaller than $\sqrt{N_R}/N_R$. The inequality $\sqrt{N_R}/N_R > \Delta N^*/N^* > \Delta N_R/N_R > \sqrt{N^*}/N^*$, derived from the above formulas and equally applicable to impulses recorded from small areas and to total count rates from the whole brain, shows that our correction for count loss leads to smaller errors than does the usual not quite accurate error estimation by $\sqrt{N_R}/N_R$. This may be seen from Table 1. The accurate measurement of the deadtime and its errors are basic requirements for this statement. The error of the deadtime has to be determined far more precisely than the statistical error of the impulse number. Deadtime (τ) was calculated according to Eq. 1 from the results of the multisource method for the scaler recording the total counts in the camera (11 μsec) and for the center of hte 1,600-word memory (23 μsec). The error of the deadtime ($\Delta\tau$) was obtained from the variance of the multisource method (0.161 μsec).

STATISTICAL SIGNIFICANCE OF CALCULATED RCBF VALUES

Some theoretical considerations suggest that the error of computed blood-flow values may well be much smaller than expected from statistical fluctuations of count rates. In general, correlations between single values constituting the washout curve may be neglected (*42*). Therefore, the propagation of the error (ΔH_i) of the i-th measured value (H_i) may be computed by applying the programs used for blood-flow calculations. The error of the final result is obtained according to the law of error propagation by varying all originally measured values (H) according to their error (ΔH). The total error (Δf) is given by

$$\Delta f = \sqrt{\Sigma \frac{\partial f}{\partial H_i}\left(\Delta H_i\right)^2}. \quad (6)$$

For this equation again the assumption of a Gaussian distribution must be accepted (*41*). It was far too complicated to calculate accurately the partial derivations in Eq. 6 for the whole experimental procedure. Therefore, a rough estimation was achieved by varying measured values (H_i) independently and observing the change in the result (f), thus giving the quantity $\partial f/\partial H_i$. To avoid the variation of 70 single values and the time-consuming computations, four representative values of the washout functions from small recorded brain areas

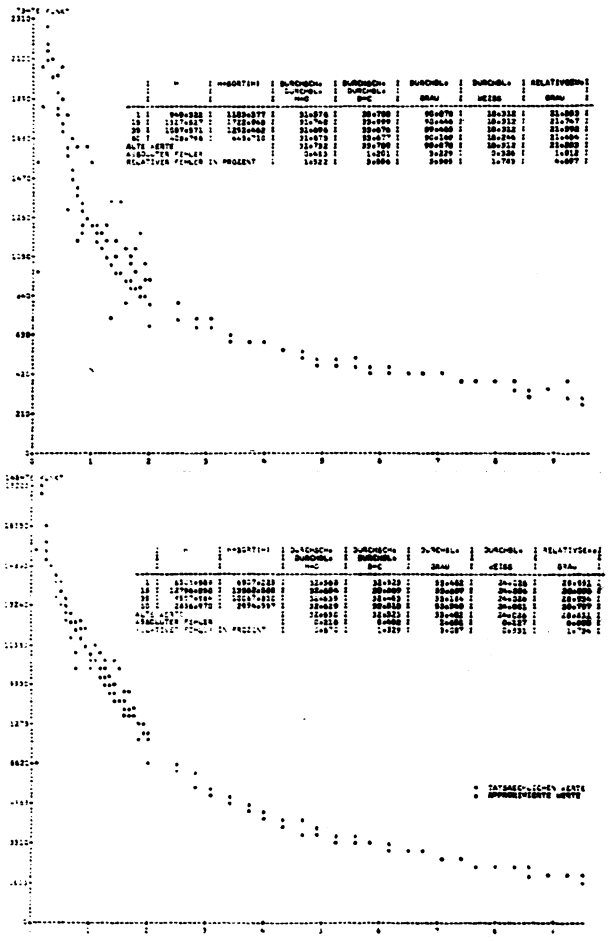

FIG. 5. Recorded count rates (indicated by asterisks) and points of fitted washout curve (indicated by dots) or activity over small brain areas of 12 × 12 mm with low (upper curve) and high count rates (lower curve). Insets show printouts of errors of blood-flow value calculated from statistical error of single count rates according to Eq. (7).

were selected and the error of rCBF values estimated from

$$\Delta f = \{3[f(H_0 + \Delta H_0) - f(H_0)]^2 + 22[f(H_{15} + \Delta H_{15}) - f(H_{15})]^2 + 20[f(H_{35} + \Delta H_{35}) - f(H_{35})]^2 + 25[f(H_{60} + \Delta H_{60}) - f(H_{60})]^2\}^{1/2}. \quad (7)$$

To reduce computing time a normal distribution of the error was assumed and the values were varied only in positive direction within the computer program.

In Fig. 5 recorded washout curves of small brain areas with different count rates are shown together with the influence of the statistical fluctuations of the single recorded values on the computed results. The count rates were sampled for short periods of time (2.4 sec for the first and second minutes, 18 sec for the third to tenth minute) and varied according to ΔH, before the conversion to counts per minute for the display in the diagram. As demonstrated in the different curves of Figs. 5 and 6, where the computed errors of the results of 75 single curves are shown in relation to the count rate over this area during the 15th sampling period of the washout curve, the size of this error depends on the number of recorded counts. Below count rates of 3,000–5,000 cpm the error is not predictable from the count rate; above this rate a close and very steep proportional correspondence exists. The knowledge of the count rate within a small brain area permits a fair estimation of the statistical error of the resulting regional blood-flow values [f_A is the flow computed according to height-over-area-method, f_G the flow in fast compartment (grey matter), f_W the flow in slow compartment (white matter), W_G the relative weight of fast flow compartment (grey matter), f_B the weighted total flow—all calculated according to bicompartmental analysis]. The flow values of two brain regions may be considered to be different, if the difference is greater than their mean-square deviation calculated according to Eq. 7. The significance of the differences between the blood-flow values of different regions may be judged by arbitrarily chosen intervals of confidence.

RELIABILITY OF RCBF VALUES

To test the reproducibility of CBF values, previous workers have applied a variety of statistical methods. Agnoli, et al (*43*) used the standard deviation of the rCBF values obtained from a control group without cerebrovascular disease to determine the range of experimental error to be expected from the technique. This figure expresses mainly physiological differences in rCBF values. Other investigators estimated the measurement error with the standard deviation of the differences between serial measurements of rCBF (*36*) or with the coefficient of variation, i.e., the standard deviation of the differences in relation to the mean of all rCBF values (*29,39*). These calculations were also done in our study using the rCBF values of serial measurements in 165 brain regions of three patients; in this material rCBF values obtained with low count rates were also included. The standard deviation due to measurement error, presented by Wilkinson, et al (*36*) as 4.6%, was 3.1% in our study. The coefficient of variation of the serial measurement was found to be 7.9%; this value is slightly higher than the values obtained with large detectors: 4.8% (*39*) and 3.6% (*29*). All these procedures give some information about the error of the measured values, but do

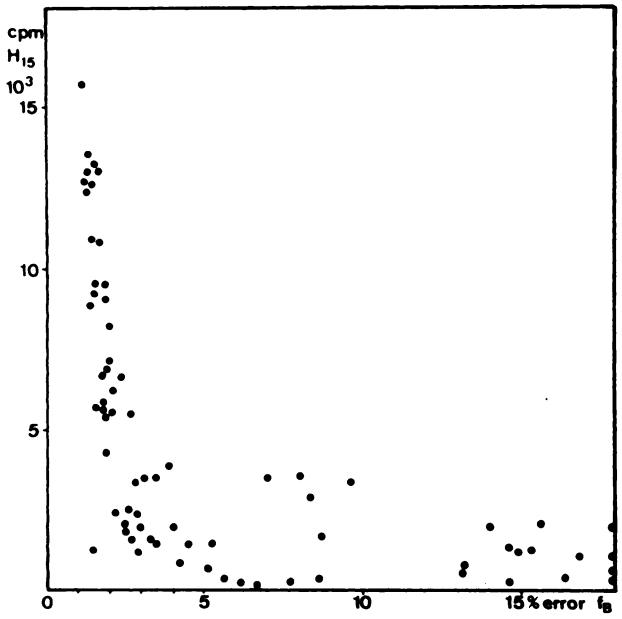

FIG. 6. Diagram of relation of error of blood-flow values (calculated according to Eq. 7) and of the count rate at 15th point of washout curve showing results of 75 single brain areas of five patients. Below height of 4,000 cpm statistical error is very variable and may be too high for valid result. Above this count rate error is close to 2%.

not yield an estimate of the predictability of a second measurement from the first. A statistical estimate of this dependency may be obtained by a regression analysis, as was done in our study.

In Fig. 7 the blood-flow values of a first (abscissa) and a second (ordinate) measurement of 165 brain regions of three different patients are shown. Assuming a normal distribution of the population of blood-flow values in different patients, a linear regression was calculated based on these results of 165 rCBF values. The good reproducibility is demonstrated by the high correlation coefficient ($r = 0.924$) and the slope of the regression line close to 1 (0.98). The constant 2.28 indicates a systematic error of the second measurement and is due to overcorrection of the background activity for the second measurement, when the isotope from the first measurement is still present in the head.

The difference between the obtained regression coefficient 0.98 and the hypothetical slope 1 was tested by the appropriate version of the student-t-test and was found to be insignificant ($t = 0.6341$, $df = 163$). The standard deviation of the dependent variable ($s_{y.x}$), estimated according to the regression equation, was found to be 4.24. This standard deviation is a means of estimating the error of the second measurement. Despite the fact that the time-dependent changes in the variable itself (spontaneous rCBF variations during the 45 min between the measurements) are combined with the technical error, this standard deviation of the dependent variable (4.24) is within the range of the value (3.49) of Agnoli, et al (*43*), who used the standard deviation of the rCBF values of a control group as an error estimate, without taking into consideration the reproducibility.

CONCLUSIONS

The reflections and results presented in this paper prove, in our opinion, that the gamma-camera 1,600-word memory system is a suitable and adequate instrument for measuring rCBF. Its features are the good spatial resolution and scatter elimination, in which points it seems to be superior to the recently used multiprobe techniques. The rCBF maps (Fig. 8), calculated from the data registered and stored by this instrument, provide many rCBF values and a clear survey of the regional flow conditions. The method is independent of the position of the detectors to the head, and no area may accidentally fail to be

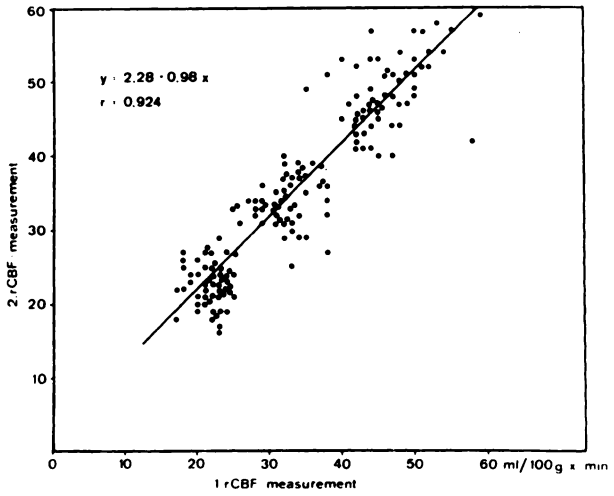

FIG. 7. Correlation of blood-flow values of first (abscissa) and second (ordinate) measurement in 165 small brain regions. Values were obtained from repeated measurements in three different patients and linear regression was calculated.

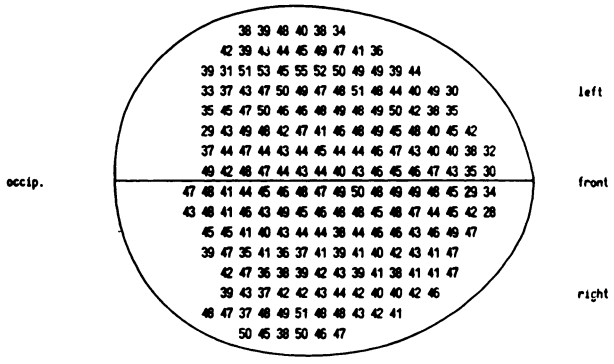

FIG. 8. RCBF map of both hemispheres in patient with transient ischemic attacks caused by stenosis of right internal carotid artery (viewed from above).

registered due to its position between single detectors.

One disadvantage of the gamma-camera system is the loss of counts with the necessary high count rates. This severe handicap was reduced by correction for count loss, justified by the positive influence of deadtime on counting statistics. Furthermore, it was demonstrated that the theoretically and empirically determined reliability of rCBF values derived from the many relatively low count rates defining a washout curve is much better than was expected using only one $\sqrt{N_R}$ as a parameter for reliability. Thus the evaluation of curves with an initial count rate of less than 5,000 cpm is reasonable, provided that the error is determined simultaneously.

All these corrections and error calculations demand a complex computer program, which is a basic requirement for a correct, exhaustive, and quick evaluation of the raw data. This has also become a requirement for multiprobe systems with more than eight probes.

Advantages and disadvantages of CBF measuring techniques are best established by comparing the results in the same group of patients. Such studies have been carried out by various authors using different methods (*11,44,47*), but a direct comparison between the gamma-camera system and the multiprobe technique is still lacking. Therefore, discussions of the properties of the individual methods are based on experiences of single investigators obtained by only one method. However, the quantification of these properties is very difficult. The importance of being able to specify the performance of the instrument used need not be stressed. The present paper is an attempt to provide this information to workers (*48–50*) now applying the gamma-camera technique for RCBF studies with or without modifications, and to others who plan to do so.

SUMMARY

A gamma camera in connection with a 1,600-word memory and a digital magnetic tape recorder is applied in order to measure regional and total cerebral blood flow. The blood-flow values are calculated by a computer, and the results are printed out in the form of blood-flow maps. For this equipment some important characteristics, such as efficiency, energy resolution and incidence of scatter, spatial resolution, count loss and counting statistics, are investigated and compared with the same parameters in a multidetector system for blood-flow studies. Apart from the count loss, the gamma-camera system is superior to the multiprobe technique. Since the error of the calculated blood-flow value is not dependent on only one single count rate but on all measurements defining the washout function, this disadvantage of the gamma camera does not limit its use for rCBF studies.

ACKNOWLEDGMENTS

We are extremely grateful to Dr. C. M. Fleck for his important help with respect to statistics and derivation of the equations and to Dr. Wenzel and the Computer Centre of the Österreichische Stickstoffwerke AG for carrying out the necessary calculations.

This work was supported by the Österreichischer Fonds zur Förderung der wissenschaftlichen Forschung and by a grant from the Österreichische Nationalbank.

REFERENCES

1. ANGER HO: Scintillation camera. *Rev Sci Instrum* 29: 27–33, 1958

2. ADAM WE, SCHENCK P, KAMPMANN H, et al: Investigation of cardiac dynamics using scintillation camera and computer. In *Medical Radioisotope Scintigraphy,* Vienna, IAEA, 1969, vol 2, pp 77–88

3. HOLROYD AM, JONES T: A simple method for obtaining dynamic quantitative information from the gamma camera. *Phys Med Biol* 14: 631–638, 1969

4. WESTERMAN B: Quantitation of the output of a scintillation camera in dynamic studies. *Phys Med Biol* 14: 39–44, 1969

5. WILKS RJ, MALLARD JR: A small gamma camera—improvements in the resolution, a setting-up procedure and a digital print-out. *Int J Appl Radiat* 17: 113–119, 1966

6. POLCYN RE, PALOYAN D, HENDRICKS KO, et al: Use of a 1600 channel analyzer with a gamma scintillation camera. In *Radioaktive Isotope in Klinik und Forschung,* Fellinger K, Höfer R, eds, München, Urban und Schwarzenberg, 1968, vol VIII, pp 11–20

7. HEISS W-D, PROSENZ P, ROSZUCZKY A, et al: A quantitative gamma camera technique. *Scan J Clin Lab Invest Supply* 102: XI:L, 1968

8. HEISS W-D, PROSENZ P, ROSZUCZKY A, et al: Die Verwendung von Gamma-Kamera und Vielkanalspeicher zur Messung der gesamten und regionalen Hirndurchblutung. *Nuclearmedizin* 7: 297–318, 1968

9. POTCHEN EJ, BENTLEY R, GERTH W, et al: A means for the scintigraphic imaging of regional brain dynamics. Regional cerebral blood flow and regional cerebral blood volume. In *Medical Radioisotope Scintigraphy,* Vienna, IAEA, 1969, vol 2, pp 577–583

10. LASSEN NA, PAULSON O: Discussion and comments to section XI on techniques for measurement of cerebral blood flow. *Scand J Clin Lab Invest Suppl* 102: XI:M, 1968

11. PAULSON OB, CRONQVIST S, RISBERG J, et al: Regional cerebral blood flow: a comparison of 8-detector and 16-detector instrumentation. *J Nucl Med* 10: 164–173, 1969

12. LASSEN NA, INGVAR DH: Radioisotopic assessment of regional cerebral blood flow. In *Progress in Nuclear Medicine,* Potchen EJ, McCready VR, eds, Basel, Karger, 1972, vol I, pp 376–409

13. INGVAR DH, LASSEN NA: Methods for cerebral blood flow measurements in man. *Brit J Anaesth* 37: 216–224, 1965

14. GLASS HJ, HARPER AM: Measurement of regional blood flow in cerebral cortex of man through intact skull. *Brit Med J* 1: 593–595, 1963

15. ANGER HO: Radioisotope cameras. In *Instrumentation in Nuclear Medicine,* Hine GJ, ed, London, Pergamon, 1967, vol I, pp 485–552

16. SVEDBERG JB: Image quality of a gamma system. *Phys Med Biol* 13: 597–610, 1968

17. CONSTABLE AR: The gamma camera. *Brit J Urol Suppl* 41: 38–45, 1969

18. ANGER HO: Sensitivity and resolution of the scintillation camera. In *Fundamental Problems in Scanning,* Gottschalk A, Beck RN, eds, Springfield, Ill, CC Thomas, 1968, pp 117–144

19. BAKER RG, SCRIMGER JW: An investigation of the parameters in scintillation camera design. *Phys Med Biol* 12: 51–63, 1967

20. WESTERMAN BR, GLASS HJ: Physical specification of a gamma camera. *J Nucl Med* 9: 24–30, 1968

21. CROUTHAMEL CE: *Applied Gamma-Ray Spectrometry.* Oxford, England, Pergamon, 1960

22. OLDENDORF WH, IISAKA Y: Interference of scalp and skull with external measurements of brain isotope content: part 2. Absorption by skull of gamma radiation originating in brain. *J Nucl Med* 10: 184–187, 1969

23. ROSS DA, ROHRER RH, HARRIS CC: Quantitative counting in the presence of coincidence-summing scintillations. *J Nucl Med* 8: 502–514, 1967

24. ROSS DA, HARRIS CC, SATTERFIELD MM, et al: Low energy gamma emiters in scanning and other clinical applications. In *Radioaktive Isotope in Klinik und Forschung,* München, Urban und Schwarzenberg, 1965, pp 108–123

25. EICHLING JO, TER-POGOSSIAN MM, RHOTEN AL: Analysis of the scattered radiation encountered in lower energy diagnostic scanning. In *Fundamental Problems in Scanning,* Gottschalk A, Beck RN, eds, Springfield, Ill, CC Thomas, 1968, pp 238–243

26. POTCHEN EJ, DAVIS DO, WHARTON T, et al: Regional cerebral blood flow in man. I. A study of the xenon 133 washout method. *Arch Neurol (Chicago)* 20: 378–383, 1969

27. ANGER HO, DAVIS DH: Gamma-ray detection efficiency and image resolution in sodium iodide. *Rev Sci Instrum* 35: 693–697, 1964

28. MALLARD JR, MYERS MJ: The performance of a gamma camera for the visualization of radioactive isotopes in vivo. *Phys Med Biol* 8: 165–182, 1963

29. MCHENRY LC, JAFFE ME, GOLDBERG HJ: Regional cerebral blood flow measurement with small probes. I. Evaluation of the method. *Neurology (Minneap)* 19: 1198–1206, 1969

30. POTCHEN EJ, DAVIS DO, WHARTON T, et al: The effect of Compton scatter on regional cerebral blood flow determination with xenon-133. *Clin Res* 15: 410, 1967

31. SCRIMGER JW, BAKER RG: Investigation of light distribution from scintillations in a gamma camera crystal. *Phys Med Biol* 12: 101–103, 1967

32. CRADDUCK TD, FEDORUK SO: An experimental determination of the overall spatial resolution of a scintillation camera. *Phys Med Biol* 10: 67–76, 1965

33. BROWNELL GL: Theory of isotope scanning. In *Medical Radioisotope Scanning,* Vienna, IAEA, 1959, pp 1–12

34. BROWNELL GL, ARONOW S, HINE GJ: Radioisotope Scanning. In *Instrumentation in Nuclear Medicine,* Hine GJ, ed, New York, Academic, 1967, vol I, pp 381–428

35. LARSSON EJ, LIDÉN K: Resolution components and differential linearity of a gamma camera. In *Medical Radioisotope Scintigraphy,* Vienna, IAEA, 1969, vol 1, pp 111–123

36. WILKINSON IMS, BULL JWD, DUBOULAY GH, et al: Regional blood flow in the normal cerebral hemisphere. *J Neurol Neurosurg Psychiat* 32: 367–378, 1969

37. FÜNFER E, NEUERT H: *Zählrohre und Szintillationszähler,* Karlsruhe, Braun, 1959

38. PRICE WJ: *Nuclear Radiation Detection,* New York, McGraw-Hill, 1964

39. HOEDT-RASMUSSEN K: Regional cerebral blood flow: The intra-arterial injection method. *Acta Neurol Scand* 43, Suppl 27: 1–79, 1967

40. EVANS RD: *The Atomic Nucleus,* New York, McGraw-Hill, 1955, p 791

41. BRANDT S: *Statistische Methoden der Datenanlyse,* Mannheim, Wien, Zürich, Bibliographisches Institut, Hochschulskripten 816/816a, 1968

42. FLECK CM, HOLZER F, SEYMANN E: Zur optimalen Information bei der Messung von Halbwertszeiten. *Nucl Instrum Meth* 94: 515–520, 1971

43. AGNOLI A, FIESCHI C, BOZZAO L, et al: Autoregulation of cerebral blood flow. Studies during drug-induced hypertension in normal subjects and in patients with cerebral vascular diseases. *Circulation* 38: 800–818, 1968

44. LASSEN NA, HOEDT-RASMUSSEN K: Human cerebral blood flow measured by two inert gas techniques. Comparison of the Kety-Schmidt method and the intra-arterial injection method. *Circ Res* 19: 681–688, 1966

45. JENSEN KB, HOEDT-RASMUSSEN K, SVEINSDOTTIR E, et al: Cerebral blood flow evaluated by inhalation of ^{133}Xe and extracranial recording: a methodological study. *Clin Sci* 30: 485–494, 1966

46. TER-POGOSSIAN MM, EICHLING JO, DAVIS DO, et al: Significance between the rCBF compartments measured by the wash-out of $H_2{}^{15}O$ and of ^{133}xenon. In *Brain and Blood Flow,* Ross Russel RW, ed, London, Pitman, 1971, pp 1–4

47. ARNOT RN, CLARK JC, GLASS HJ: Investigation of 127 xenon as a tracer for the measurement of regional cerebral blood flow. In *Brain and Blood Flow,* Ross Russel RW, ed, London, Pitman, 1971, pp 16–21

48. KLASSEN AC, RESCH JA, LOKEN MK, et al: Cerebral circulation studies using inhaled 133-xenon and the gamma camera. *Stroke* 1: 7–13, 1970

49. BELL RL, MATTHEWS N, ERICSSON AD, et al: Quantitative cerebral blood flow with the gamma camera and magnetic tape: a comparative study of intracarotid injection of ^{133}Xe and of ^{99m}Tc-pertechnetate. *J Nucl Med* 12: 338, 1971

50. TORIZUKA K, HAMAMOTO K, MORITA R, et al: Regional cerebral blood flow measurement with ^{133}Xe and scinticamera. *J Nucl Med* 12: 401–402, 1971